

Impact of surface coating and environmental conditions on the fate and transport of silver nanoparticles in the aquatic environment

Ellis, Laura-Jayne; Valsami-Jones, Eugenia; Baalousha, Mohammed ; Lead, Jamie

DOI:

[10.1016/j.scitotenv.2016.05.199](https://doi.org/10.1016/j.scitotenv.2016.05.199)

License:

Creative Commons: Attribution-NonCommercial-NoDerivs (CC BY-NC-ND)

Document Version

Peer reviewed version

Citation for published version (Harvard):

Ellis, L-J, Valsami-Jones, E, Baalousha, M & Lead, J 2016, 'Impact of surface coating and environmental conditions on the fate and transport of silver nanoparticles in the aquatic environment', *Science of the Total Environment*, vol. 568, pp. 95-106. <https://doi.org/10.1016/j.scitotenv.2016.05.199>

[Link to publication on Research at Birmingham portal](#)

Publisher Rights Statement:

Checked 14/6/2016

General rights

Unless a licence is specified above, all rights (including copyright and moral rights) in this document are retained by the authors and/or the copyright holders. The express permission of the copyright holder must be obtained for any use of this material other than for purposes permitted by law.

- Users may freely distribute the URL that is used to identify this publication.
- Users may download and/or print one copy of the publication from the University of Birmingham research portal for the purpose of private study or non-commercial research.
- User may use extracts from the document in line with the concept of 'fair dealing' under the Copyright, Designs and Patents Act 1988 (?)
- Users may not further distribute the material nor use it for the purposes of commercial gain.

Where a licence is displayed above, please note the terms and conditions of the licence govern your use of this document.

When citing, please reference the published version.

Take down policy

While the University of Birmingham exercises care and attention in making items available there are rare occasions when an item has been uploaded in error or has been deemed to be commercially or otherwise sensitive.

If you believe that this is the case for this document, please contact UBIRA@lists.bham.ac.uk providing details and we will remove access to the work immediately and investigate.

1 **Impact of Surface Coating and Environmental Conditions on the Fate and**
2 **Transport of Silver Nanoparticles in the Aquatic Environment**

3

4 **Laura-Jayne. A. Ellis¹, Eugenia Valsami-Jones¹, Jamie. R. Lead^{1,2*}, and**
5 **Mohammed Baalousha^{2*},**

6

7 ¹*School of Geography, Earth and Environmental Sciences, University of Birmingham, Edgbaston,*
8 *Birmingham, B15 2TT, U.K.*

9 ²*Center for Environmental Nanoscience and Risk (CENR), Department of Environmental Health*
10 *Sciences, Arnold School of Public Health, University of South Carolina, Columbia, 29208, USA.*

11 *Corresponding Authors: Jlead@mailbox.sc.edu and Mbaalous@mailbox.sc.edu

12

Content	Page
Highlights	2
Abstract	2
1 Introduction	4
2 Materials and Methods	6
2.1 Materials	6
2.2 Synthesis and Characterization of AgNPs	6
2.3 Microcosm Experiments	8
2.4 Modeling the transport of Ag	9
3 Results and Discussion	11
3.1 Behavior and Transport of PVP-AgNPs	11
3.1.1 Behavior of PVP-AgNPs in UPW	17
3.1.2 Behavior of PVP-AgNPs in MHW	18
3.1.3 Behavior of PVP-AgNPs in MHW-SRFA	19
3.2 Behavior and transport of cit-AgNPs	20
3.2.1 Behavior of cit-AgNPs in UPW	24
3.2.2 Behavior and transport of cit-AgNPs in MHW	25
3.2.3 Behavior of cit-AgNPs in MHW-SRFA	28
4 Conclusions	30
Acknowledgments	31
References	32

13

14

15

16

17

18 |

19

20 | Highlights
21 |

- 22 • Aquatic microcosms were used to study the transport and behavior of
23 AgNPs in model low and high ionic strength waters.
- 24 • Surface coating and solution chemistry has a major impact on AgNP
25 stability.
- 26 • UV-Visible spectrophotometry provided important information on the aggregation
27 and migration of the AgNPs.
- 28 • Experiments showed that PVP-coated AgNPs migrate via diffusion in all
29 conditions, whereas citrate-coated AgNPs follow both sedimentation and
30 diffusion dependent upon the aquatic environments.

31 **Abstract**

32 The role of surface coating (polyvinylpyrrolidone (PVP) and citrate) and water
33 chemistry on the fate and behaviour of AgNPs in aquatic microcosms is reported in
34 this study. The migration and transformation of the AgNPs was examined in low
35 (ultrapure water- UPW) and high ionic strength (moderately hard water – MHW)
36 preparations, and in the presence of modelled natural organic matter (NOM) of
37 Suwannee River Fulvic Acid (SRFA). The migration and fate of the AgNPs in the
38 microcosms was validated using a sedimentation-diffusion model and the
39 aggregation behaviour was monitored by UV-visible spectrometry (UV-vis).
40 Dissolved and particulate Ag concentrations (% Ag) were analyzed by ultrafiltration
41 methods. Imaging of the AgNPs was captured using transmission electron
42 microscopy (TEM).

43 Results indicate that PVP-coated AgNPs (PVP-AgNPs) remained stable for 28
44 days with similarly distributed concentrations of the PVP-AgNPs throughout the
45 columns in each of the water conditions after approximately 96 hours (4 days). The
46 sedimentation-diffusion model confirmed PVP-AgNP stability in each condition, by
47 showing diffusion dominated transport by using the original unaltered AgNP sizes to
48 fit the parameters. In comparison, citrate AgNPs were largely unstable in the more
49 complex water preparations (MHW). In MHW, aggregation dominated behavior
50 followed by sedimentation/dissolution controlled transport was observed. The
51 addition of SRFA to MHW resulted in small stabilizing effects, to the citrate coated
52 AgNPs, producing smaller sized AgNPs (TEM) and mixed sedimentation and
53 diffusion migration compared the studies absent of SRFA. The results suggest that

54 surface coating and solution chemistry has a major impact on AgNP stability,
55 furthermore the corresponding modeling will support the experimental understanding
56 of the overall fate of AgNPs in the environment.

57

58

59

60 |

61

62 **1 Introduction**

63 Silver nanoparticles (AgNPs) are commercially exploited for their antibacterial
64 and other properties(Benn and Westerhoff 2008)(Piccinno, Gottschalk et al. 2012).
65 Although there are uncertainties, some studies have found AgNPs to be potentially
66 toxic(Fabrega, Luoma et al. 2011) with adverse effects on biota(Navarro, Baun et al.
67 2008). Due to their extensive use in consumer products, it is also inevitable that
68 AgNPs will enter the aquatic environment(Benn and Westerhoff 2008).
69 Environmental fate and exposure models indicate that the predicted environmental
70 concentrations (PECs) of AgNPs in surface waters will be in the range of ng to $\mu\text{g L}^{-1}$
71 (Gottschalk, Sun et al. 2013). The quantities of NPs and rates of release will
72 influence environmental concentrations, and be heavily impacted by their
73 environmental behavior and transformations(Dale, Casman et al. 2015). The fate of
74 the NPs is determined by key processes such as dissolution, aggregation,
75 sedimentation, deposition, and sulfidation<sup>(Lowry, Gregory et al. 2012),(Peijnenburg, Baalousha et al.
76 2015)</sup>. These processes are largely influenced by the chemical complexity of the
77 aquatic system such as ionic strength, pH and natural organic matter (NOM), and
78 also the nature of the NPs(Peijnenburg, Baalousha et al. 2015). Deposition of AgNPs
79 onto solid surfaces will reduce the migration of the AgNPs in suspension and
80 influence their long term fate in the environment (Bae et al, 2013). Aggregation will
81 increase particle size, reduce surface area and influence dissolution(Hotze, Phenrat
82 et al. 2010) resulting in settling and sedimentation dominated migration which is a
83 likely pathway for AgNPs. However, it has also been suggested that AgNPs can be
84 modified by NOM leading to prolonged persistence in surface waters(La Farre, Pérez
85 et al. 2008). Furthermore, capping agents are designed to increase colloidal stability
86 of the AgNPs by reducing the surface energy(Ju-Nam and Lead 2008), which
87 prevent interactions with the surrounding environment and avoid NP-NP interactions
88 reducing aggregation rates(Kvitek, Panáček et al. 2008).

89 For charge stabilized-AgNPs, low ionic strength and high concentrations of NOM
90 minimize homoaggregation(Chinnapongse, MacCuspie et al. 2011), whereas high
91 ionic strength usually causes significant aggregation, even in the presence of high
92 NOM concentrations most likely as a result of bridging mechanisms by divalent
93 cations^{(Baalousha, Nur et al. 2013),(Chen and Elimelech 2007)}. However, sterically-stabilized AgNPs
94 are generally more stable than charge-stabilized NPs and are less likely to undergo

95 aggregation and sedimentation, even at high ionic strengths^{(Baalousha, Arkill et al.}
96 2015),(Hitchman, Smith et al. 2013) and often less prone to dissolution.

97 The aim of the current study is to produce a model to validate the environmental
98 fate and migration behavior of AgNPs by investigating their behavior in static water
99 'microcosms'. In particular, this paper reports the impact of water chemistry and
100 AgNP surface coating (citrate and PVP) on the fate of AgNPs over a period of 28
101 days. The concentration and aggregation behavior of AgNPs were measured by
102 atomic absorption spectroscopy (AAS) and UV-visible spectrophotometry (UV-vis).
103 The measured Ag concentrations were fitted using a diffusion-sedimentation
104 model^{(Hinderliter, Minard et al. 2010),(Socolofsky and Jirka 2005)} to illustrate the dominant fate
105 processes (e.g. aggregation and sedimentation, or diffusion) controlling the fate of
106 Ag NPs in a range of synthetic waters from pure water to moderately hard water
107 spiked with fulvic acid as a surrogate of natural organic matter.

108
109

110 **2 Materials and Methods**

111 *2.1 Materials*

112

113 Commercially available chemicals and solvents were purchased from Sigma-
114 Aldrich (Dorset, UK) and were of analytical reagent grade. Ultra pure water (UPW)
115 with a maximum resistivity of $18.2 \text{ M}\Omega\text{cm}^{-1}$ was used throughout the experiments.
116 Suwannee River fulvic acid (SRFA) was purchased from the International Humic
117 Substances Society (IHSS, St. Paul, MN, USA). Atomic force microscopy (AFM)
118 cantilevers were purchased from Park systems corp, Suwon, Korea and used for
119 AFM analysis. More information about the materials used in this experiment is
120 provided in the supporting information (Table SI.1).

121

122 *2.2 Synthesis and Characterization of AgNPs*

123

124 Citrate-coated silver nanoparticles (cit-AgNPs) were synthesized by following a
125 published methodology (Cumberland and Lead 2009) using reagent grade chemicals
126 shown in table SI.1. Briefly, a 100 mL (0.25 mM) silver nitrate (AgNO_3) solution was
127 mixed with a 100 mL (0.25 mM) sodium citrate solution, followed by addition of 6 mL
128 (0.25 mM) sodium borohydride (NaBH_4). The mixture was then heated at 100°C for
129 2 hours, while stirring vigorously. The resulting suspension was then refrigerated
130 overnight at 4°C and purification was carried out using a Millipore stirred cell
131 ultrafiltration (1 kDa) system under nitrogen gas. PVP-AgNP suspensions (Tejamaya,
132 Römer et al. 2012) were prepared by cooling a solution of (2 mM) NaBH_4 and PVP
133 (M_w 10000, Sigma Aldrich) to 4°C . AgNO_3 (1 mM) was added to the suspension
134 dropwise with vigorous stirring. The suspensions were refrigerated overnight at 4°C .
135 Ultrafiltration using a Millipore stirred ultrafiltration cell with a cellulose membrane of
136 1 kDa (purchased from Sigma) under nitrogen (N_2) gas at approx 14 PSI was
137 performed to remove Ag ions.

138 A multi-method approach was used to characterize the AgNPs, both 'as
139 prepared AgNPs' and samples withdrawn from the microcosm. Dynamic light
140 scattering (DLS), was used to measure hydrodynamic size using a Malvern
141 Nanosizer 5000. Particle core size was measured by transmission electron
142 microscopy (TEM, particle equivalent circular diameter) and AFM (particle height).

143 Samples were prepared by drop casting methods by depositing a 20 μL drop of
144 AgNP suspension on a 300 mesh carbon-coated copper TEM grid (Agar Scientific,
145 UK) for TEM analysis, and a freshly cleaved mica sheet for AFM analysis. The AgNP
146 suspension drop was left for approximately 30 minutes to allow the NPs to adhere to
147 the carbon membrane coating the TEM grid and the mica sheets for AFM. Both the
148 TEM grids and the mica sheets were then rinsed with UPW to remove excess water,
149 avoid NP aggregation and salt crystallization(Baalousha and Lead 2012).

150 All TEM analyses were performed using a JEOL 1200EX 100kv Max system or a
151 Tecnai F20 Field Emission gun (FEG) TEM coupled with an X-ray energy dispersion
152 spectroscopy (EDS) detector from Oxford Instruments. For each sample, a minimum
153 of 100 particles from different randomly selected sample areas of multiple grids,
154 were used to calculate the size and shape measurements using Digital Micrograph
155 software (Gatan Inc, Pleasanton, CA, USA). The measured sizes were then
156 classified into intervals of 0.5 nm to construct particle size distribution histograms.

157 All AFM analyses were performed using an XE-100 AFM (Park systems Corp.,
158 Suwon, Korea). The measurements were carried out in true non-contact mode using
159 a Silicon cantilever with a typical spring constant of 42 N m^{-1} (PPP-NCHR, Park
160 systems Corp., Suwon, Korea). All scans were performed at ambient conditions,
161 which have been shown to produce accurate sizing, despite loss of most, but not all
162 water^{(Baalousha and Lead 2013),(Balnois and Wilkinson 2002)}. Images were recorded in topography
163 mode with a pixel size resolution of 256×256 and a scan rate of 0.5-1.0 Hz. Height
164 measurements of the AgNPs were made using the transect analysis using the XEI
165 data processing and analysis software of the microscope (Park Systems Corp.,
166 Suwon, Korea). For each sample, a minimum of 100 height measurements were
167 performed, which are sufficient to produce a representative particle size
168 distribution(Baalousha and Lead 2012). The measured heights were then classified
169 into intervals of 0.5 nm to construct particle size distribution histograms.

170 Total silver (Ag) concentrations were measured by flame atomic absorption
171 spectroscopy (FAAS) using a Perkin Elmer instrument AAnalyst 300, with an air-
172 acetylene mixture. Limits of FAAS instrumentation detection were devised by running
173 a set of blanks (ultrapure water) which were measured at $2 \pm 2 \mu\text{g L}^{-1}$ and a set of
174 standards to determine a concentration of $50 \mu\text{g L}^{-1}$. The concentrations of AgNPs in
175 the purified NP suspensions were 11 mg L^{-1} and 20 mg L^{-1} for the cit- and PVP-
176 AgNPs, respectively.

177 The surface plasmon resonance (SPR) of AgNP suspensions was measured
 178 using a Jenway 8300 double beam UV-visible spectrometer (UV-vis) over the
 179 wavelength range of 300-800 nm, with the use of suitable controls (UPW and MHW
 180 water). A 10 cm long path length cuvette was used to collect spectra. Full details of
 181 AgNP properties are provided in Table 1 and Figures S1-S9 in the Supporting
 182 Information.

183

184 Table 1: Properties of the 'as-prepared' AgNPs obtained using a multi-Method Characterisation approach

Technique	Citrate AgNPs	PVP AgNPs
Particle core size measured by TEM (nm)	11 ± 3	11 ± 2 nm
Particle height measured by AFM (nm)	12 ± 3	11 ± 3
z-average hydrodynamic diameter measured by DLS (nm)	21 ± 2	20 ± 2
Polydispersity index measured by DLS (PDI)	0.10 ± 0.04	0.20 ± 0.04
Ag concentration FAAS (Concentration mg L ⁻¹)	11.5 ± 1	20.0 ± 2

185 *Key to annotations: TEM: transmission electron microscopy, AFM, atomic force microscope, DLS: dynamic light
 186 scattering, FAAS: flame atomic absorption spectrometer

187

188 2.3 Microcosm Experiments

189

190 The fate and behavior of AgNPs was assessed in aquatic microcosms. The
 191 microcosms are cylindrical columns made of polystyrene plastic and measuring 100
 192 cm in height, 25 cm in diameter and 43 L in volume. The columns were shielded
 193 from light in all experiments, by wrapping the exterior walls in foil. AgNPs were
 194 introduced as a single concentration pulse through a mesh at a depth of 5 cm below
 195 the surface water (Figure SI.12). The starting mass of AgNPs (M_{Ag}) added to the
 196 columns (4.3 mg) was estimated to give a final concentration of 100 $\mu\text{g L}^{-1}$ Ag,
 197 assuming uniform distribution of Ag throughout the water column and no losses. This
 198 Ag mass was introduced as 390 ml of 11 mg L^{-1} cit-Ag NPs, or 215 ml of 20 mg L^{-1}
 199 PVP-Ag NPs. The concentration of AgNPs was selected to be as close as possible
 200 to predicted environmental concentrations of AgNPs⁵, while maintaining sufficient
 201 particle concentration to enable analysis. To determine the minimum detectable
 202 concentration of AgNPs by UV-vis spectra were collected on AgNPs following serial
 203 dilutions, which suggested that a minimum concentration of 50 $\mu\text{g L}^{-1}$ was required
 204 for detection (Figure SI.10). The fate and transport of AgNPs was investigated in
 205 three media: 1) UPW, 2) EPA moderately hard water (MHW), and 3) EPA
 206 moderately hard water spiked with 1 mg L^{-1} Suwannee River fulvic acid (MHW-

207 SRFA). For lakes and surface waters the expected total organic carbon ranges
208 between 1-30 mg L⁻¹, depending on the trophic state (Hendricks 2006, Thurman
209 2012). As lower concentrations are more frequent, it was decided that the
210 concentration would be at the lower end of the scale at 1 mg L⁻¹.

211 All microcosm experiments were performed in triplicate. The MHW was
212 prepared according to guidelines from the United States Environmental Protection
213 Agency (US EPA, 2002) (Table SI.2). The MHW-SRFA was prepared by adding
214 SRFA stock to the MHW and leaving for 24 hours.

215 Water samples of 5 mL were collected at the introduction point (water surface),
216 middle (50 cm from the surface and bottom), and bottom (90 cm from the surface) of
217 the microcosm column. Water samples were collected using six inch stainless steel
218 hypodermic needles which were permanently fixed to the sampling points. The
219 sampling point at the bottom was always sampled at a 45° angle downwards in order
220 to obtain samples that were within 1 cm of the bottom of the microcosm. No mixing
221 was performed and mesocosms were kept at room temperature (21 ± 2°C). Water
222 samples were collected at different time points following introduction of Ag NPs; 0,
223 0.5, 1.5, 3.5, 5.5, and 8 hours on day 1 and then on daily-basis for the first 14 days,
224 then again on days 21 and 28. Additionally, samples from the surface and bottom
225 were analysed on days 1-14, 21 and 28, to assess the dissolved and particulate
226 concentration (% Ag) using ultrafiltration methods using a Millipore stirred
227 ultrafiltration cell with a cellulose membrane of 1 kDa (purchased from Sigma) under
228 nitrogen (N₂) gas at approx 14 PSI. Ultrafiltration membrane viability tests were
229 performed by running a set of known standards and checking their recovery rates, by
230 measuring the Ag concentration in the retained and filtrate content. Thus, any
231 adsorbed Ag to the membrane was accounted for in the recovery calculations. All
232 water samples were analyzed for total Ag concentrations by atomic absorption
233 spectroscopy (AAS), and for AgNP aggregation by UV-vis(Baalousha, Nur et al.
234 2013) and confirmed by TEM analysis.

235

236 *2.4 Modeling the transport of Ag*

237

238 As the water in the column was kept stagnant throughout, the transport of AgNPs in
239 the microcosms is determined by their sedimentation after aggregation and their

240 diffusion. These transport processes can be modeled by the diffusion-sedimentation
 241 equation(Socolofsky and Jirka 2005) (Eq 1).

$$242 \left| \frac{\partial C}{\partial t} + \frac{\partial \mu_i C}{\partial x_i} = D \frac{\partial^2 C}{\partial x_i^2} \right. \quad [\text{Eq 1}]$$

243
 244 Where D is the diffusion coefficient ($\text{m}^2 \text{s}^{-1}$) of the AgNPs or their aggregates, C is
 245 concentration (mg L^{-1}), t is time following AgNP introduction, viscosity of the solution
 246 μ (Pa.s), and x is the distance AgNPs travelled into the column from the introductory
 247 point. To calculate Ag concentration profile as a function of time at the sampling
 248 point in the water column, we used a simple analytical solution for Eq 1 that satisfies
 249 the experimental boundary conditions. These boundary conditions are: 1) absence of
 250 AgNPs in the water column at $t = 0$; that is $C_{\text{Ag}} = 0$ at $t = 0$ for $0 < x < L$, 2)
 251 introduction of AgNPs at the top of the water column; that is $C_{\text{Ag}} = C_0$ at $t = 0$ and x
 252 $=0$, and 3) no flux at the bottom of the column; that is $dC/dx = 0$, at $x=L$. Using these
 253 boundary conditions, the analytical solution of Eq 1 can be given by Eq 2:

$$254 \left| C(x, t) = \frac{M}{A\sqrt{4\pi Dt}} \left(\exp\left(-\frac{(x-x_0)^2}{4Dt}\right) + \exp\left(\frac{(x-x_1)^2}{4Dt}\right) \right) \right. \quad [\text{Eq 2}]$$

255
 256
 257 Where x_0 is the point where the NPs are introduced to the column, A is column cross
 258 section area, and M is the mass of the introduced AgNPs. The nanoparticle diffusion
 259 coefficient and sedimentation velocity can be described by Stokes-Einstein (Eq 3)
 260 and Stokes equation(Hinderliter, Minard et al. 2010) (Eq 4):

$$261 \left| D = \frac{kT}{3\pi\mu d} \right. \quad [\text{Eq 3}]$$

$$262 \left| U = \frac{g(\rho_p - \rho_f)d^2}{18\mu} \right. \quad [\text{Eq 4}]$$

263
 264 Where k is Boltzman constant ($\text{m}^2 \text{kg s}^{-2} \text{K}^{-1}$), T is temperature (K), μ is medium
 265 viscosity ($\text{kg m}^{-1} \text{s}^{-1}$) and d is particle diameter (m). The sedimentation velocity is U
 266 (m s^{-1}), g is the gravitational force (m s^{-2}), particle density is ρ_p (kg m^{-3}) and fluid
 267 density is ρ_f , (Hinderliter, Minard et al. 2010). These constant values are described in
 268 Table 2.

269
 270

271
272
273
274
275

Table 2: Constant values used in the model

Unit	Constant value	Description
g	9.81	Acceleration of gravity (m s^{-2})
Pp	10490	Density of the particle (kg m^{-3})
Pf	998	Density of the medium (kg m^{-3})
K	1.38065×10^{-23}	Boltzman constant ($\text{m}^2 \text{kg s}^{-2} \text{K}^{-1}$)
T	293.15	Temperature $^{\circ}\text{K}$
μ	0.001	Viscosity of medium (Pa.s) = $\text{kg (m}^{-1}\text{s}^{-1})$

276
277

278 This analytical solution can only be used to predict the concentration of AgNPs in the
279 water phase and does not account for particle accumulation at the bottom of the
280 mesocosm following sedimentation/settling on the microcosm floor. Additionally, this
281 analytical solution accounts only for NP diffusion and sedimentation and does not
282 take into account AgNP dissolution and losses of Ag due to sorption on to the solid
283 wall surfaces. Therefore, discrepancies between data and model can be explained
284 partially by dissolution and sorption. The measured concentrations were then fitted
285 using Eq 2, which is essentially an analytical solution of the diffusion-sedimentation
286 model (Eq 1). The fitting parameters that changed were the particle size and
287 concentration, and the rest of the values remained constant.

288

289 The weighted sum of squared errors was calculated using Eq 5:

290
$$X^2 = \sum \frac{(O-E)^2}{\sigma^2} \quad [\text{Eq 5}]$$

291 Where σ^2 is the variance of the measured Ag concentrations, O is the observed
292 concentration data, and E is the expected Ag concentration data. The fitting
293 parameters (nanoparticle diameter and mass of Ag introduced to the water column)
294 were optimized by Solver software in Microsoft Excel by minimizing the weighted
295 square error. The middle point data were used in the fitting process as these
296 concentrations are likely to be most accurate concentrations. The top sampling point
297 can be affected by mixing with the water in the introduction reservoir, whereas the
298 bottom sampling point concentrations could be impacted by particle sedimentation.

299

300 **3 Results and Discussion**

301

302 **3.1 Behavior and Transport of PVP-AgNPs**

303

304 In all media, PVP-AgNP behaviour followed a pattern broadly consistent with
305 diffusion dominated transport (Tejamaya, Römer et al. 2012). The Ag concentration
306 profiles in UPW, MHW and MHW-SRFA for each of the three sampling points are
307 presented in Figure 1. As described above (section 2.3), all microcosms were spiked
308 with a total mass of Ag NPs that should result in a final concentration of $100 \mu\text{g L}^{-1}$
309 Ag in the water column, assuming uniform distribution of Ag throughout the water
310 column and no losses. The total Ag concentration profiles in figures 1A, 1D and 1G,
311 in each water condition, show that the average maximum concentration at the
312 surface sampling point reaches $50 \pm 5 \mu\text{g L}^{-1}$ after 120 hours, where it remains
313 constant for the duration of the study. Time 0 represents the first 5 minutes after
314 sample introduction due to the time taken to sample each depth and microcosm
315 column. This time lapse accounts for the low concentrations of Ag detected at time 0
316 in both the middle (Figures 1b, 1E and 1H) and bottom sampling points (Figures 1C,
317 1F, and 1I). Due to the immediate mixing of the AgNPs on introduction, it is possible
318 for the rapid diffusion of ionic species, which would account for the measured small
319 Ag concentrations in the lower depths at time 0. On the other hand, particle
320 dispersion is a much slower process (as shown by the higher concentrations of Ag
321 held in the surface water up to 96 hours, and as a result, after ca. 50 hours, both the
322 middle and bottom sampling points show the total Ag concentration increased to
323 reach a plateau of $50 \pm 15 \mu\text{g L}^{-1}$. It may thus be concluded that the behavior is the
324 same throughout the microcosm columns and conditions, showing losses of
325 approximately 50-70 % from the expected $100 \mu\text{g L}^{-1}$ Ag concentration. In addition to
326 the analytical limitations, losses of Ag may have occurred from the sorptive losses of
327 the AgNPs to the walls. The total Ag concentration profiles were also fitted with Eq 2
328 to produce a predicted concentration over time based on particle size and the mass
329 of Ag introduced to the water column (M_{Ag}) (Figures 1 and Table 3). The parameters
330 were based on particle sizes between 11 and 20 nm. The M_{Ag} was between 1.4 and
331 2.4 mg to reflect the range of concentrations resulting from losses as previously
332 discussed during sampling (especially from areas of high concentration) and

333 sorption. Ultrafiltration was used as a qualitative measure of the proportion of AgNP
334 transformations in the surface and bottom depths. Ionic Ag (Ag^+) and AgNP data is
335 presented in the supporting information (Tables SI.3, SI.5 and SI.7). In all conditions,
336 over the 28 day study period, PVP-AgNPs accounted for at least 75% of the total Ag
337 concentration in the surface water and 70% in the bottom depth.

338

339

340

341

342

343

344

345

346

347

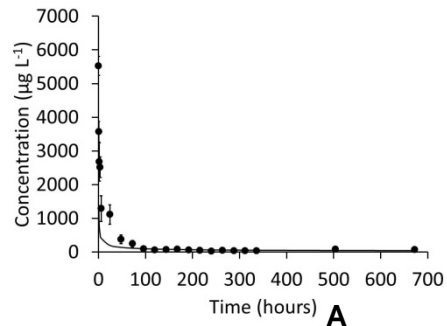
348

349

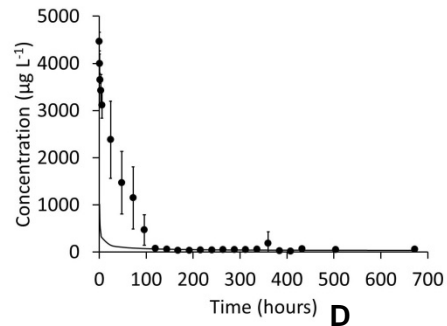
350

351

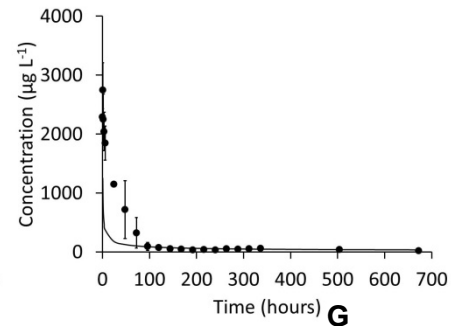
UPW



MHW

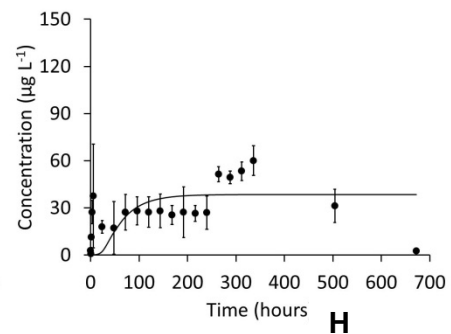
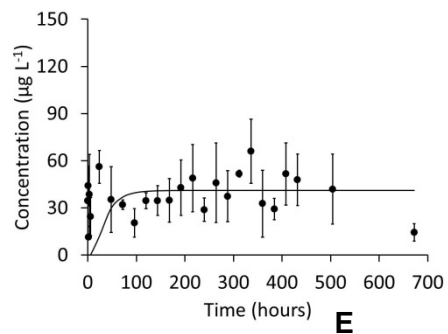
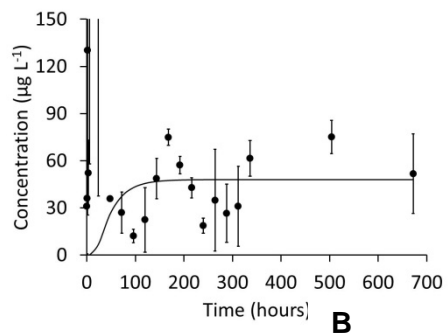


MHW SRFA



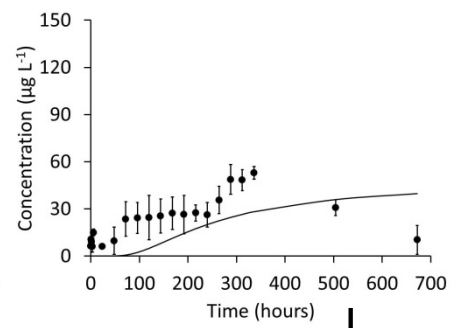
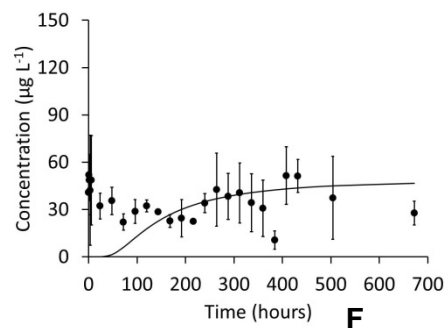
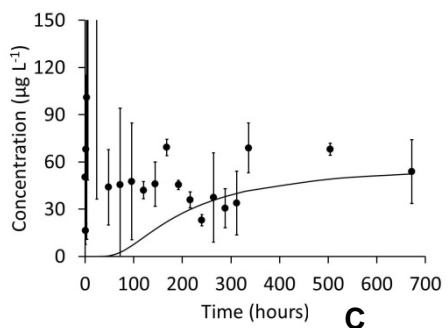
352

Surface



353

Middle



354

Bottom

— Modelled Ag Concentration ● Total Ag Concentration

356

357

358

359

360

361

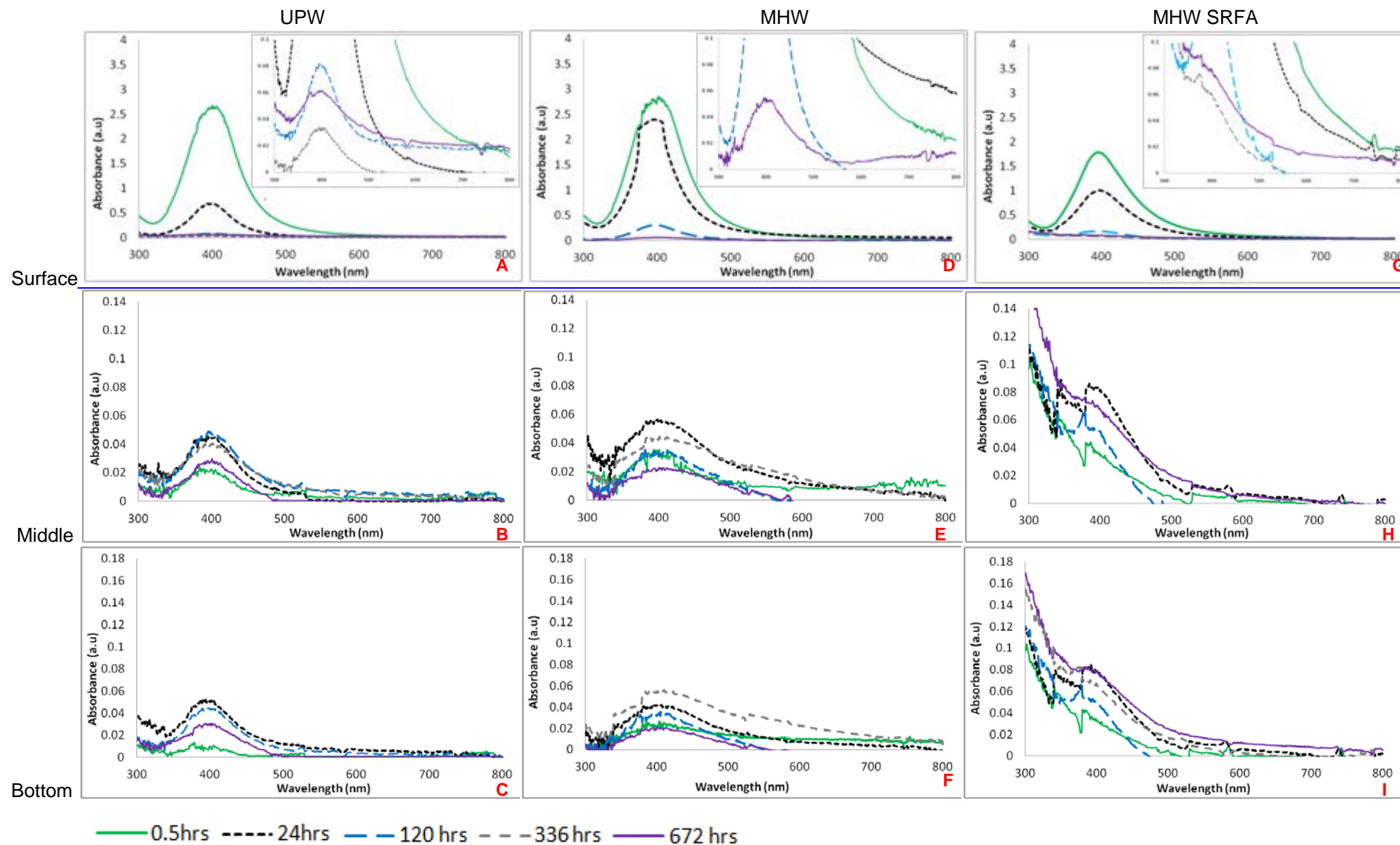
Figure 1: Observed and modelled total Ag concentrations over time for the PVP AgNP study in the surface, middle and bottom depths of the mesocosm, in each of the water conditions (parameters in supporting information) A) UPW surface water, B) UPW middle depth water, C) UPW bottom depth water, D) MHW surface water, E) MHW middle depth water, F) MHW bottom depth water, G) MHW SRFA surface water, H) MHW SRFA middle depth water and I) MHW SRFA bottom depth water. Dots show the average concentrations of three independent triplicates, error bars represent the standard deviation of the measured concentrations in the three replicated and the solid lines is the fitted model. Mass of Ag NPs introduced to the column fixed at 4.3 mg.

362
363
364
365
366
367
368
369
370
371
372
373
374
375
376
377
378
379
380
381
382
383
384
385
386
387
388
389
390
391
392
393
394
395

Collectively, all the UV-vis spectra for the PVP-AgNPs (Figure 2) show one uniform peak centered on 400 nm, comparable to the ‘as prepared PVP-AgNPs (Figure SI.1) and is indicative of unaltered AgNPs^{(Tejamaya, Römer et al. 2012),(Römer, White et al. 2011)}. The differences in the UV-vis absorbance maximum (λ_{max}) was also used to trace AgNP movement throughout the microcosms, showing as the λ_{max} absorbance decreased over time from the surface sampling point, the λ_{max} increased in the middle and bottom areas, indicating the migration of PVP-AgNPs into the column. The migration of PVP-AgNPs corresponds with the time trends shown in the modeled and observed Ag concentration data (Figure 1), as the AgNPs move through the microcosm. Losses and reduction in SPR spectra can also be used to indicate dissolution of AgNPs when total Ag concentrations remain unchanged. In all cases the SPR was still detectable at each sampling point at the end of the 28 day study showing particle presence.

To provide further understanding of the PVP-AgNP fate behavior, TEM analysis was conducted on samples of PVP-AgNPs collected from the surface and bottom sampling areas at selected time intervals (Figure 3). All reported TEM sizes were consistent with our experimental data and in agreement with the average particle sizes within the error of measurements and high diffusion coefficients compared to settling velocities (Table 3) used to fit the model data for each water condition.

396
397



398

399

400

401

402

403

404

Figure 2: comparison SPR profiles of PVP AgNP over time for the surface, middle and bottom depths of the mesocosm, in each of the water conditions, A) UPW surface water, B) UPW middle depth water, C) UPW bottom depth water, D) MHW surface water, E) MHW middle depth water, F) MHW bottom depth water, G) MHW SRFA surface water, H) MHW SRFA middle depth water and I) MHW SRFA bottom depth water.

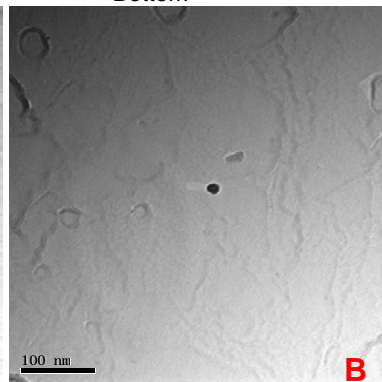
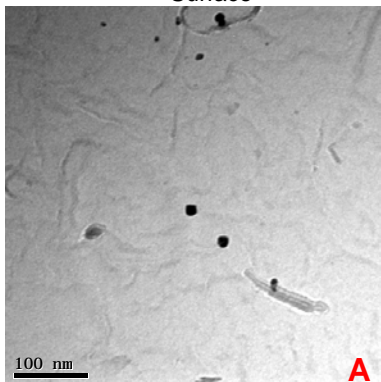
405

Surface

Bottom

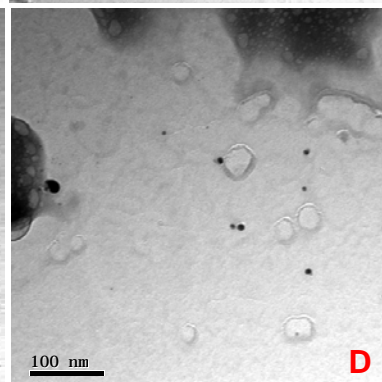
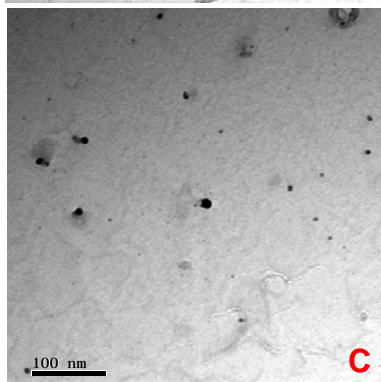
406

UPW



407

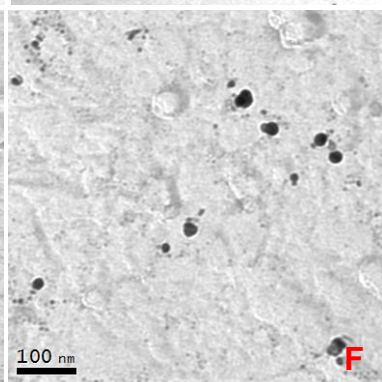
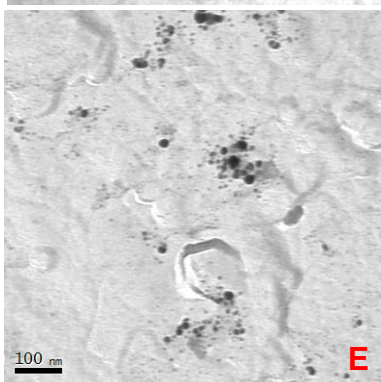
MHW



408

409

MHW SRFA



410

411

Figure 3: TEM imaging of PVP AgNPs recovered after 24 hours in each of the water conditions, A) surface UPW, B) bottom UPW, C) surface MHW, D) bottom MHW, E) surface MHW SRFA and F) bottom MHW SRFA.

412 Table 3. Silver mass, diameter, diffusion coefficient and settling velocity calculated by fitting the measured concentration using the
 413 diffusion-sedimentation equation

	M_{Ag} (mg)	d (nm)	D ($10^{-12} \text{ m}^2\text{s}^{-1}$)	U_s (10^{-8} m s^{-1})
PVP-Ag NPs				
UPW	2.4	20	21.5	0.21
MHW	2.0	14.8	28.9	0.11
MHW-SRFA	1.4	11	39	0.06
Cit-Ag NPs				
UPW	4.0	10.0	43	0.05
MHW	2.0	88.4	4.9	4.0
MHW-SRFA	3.2	12.7	33.7	0.08

414 M_{Ag} mass of Ag introduced to the water column (mg), D diffusion coefficient, v settling velocity, d diameter (nm)

415

416

417 3.1.1 Behavior of PVP-AgNPs in UPW

418

419 To assess the stability and migration behavior of the PVP-AgNPs in UPW the model
 420 parameters were optimized using the weighted sum of squared errors (Eq 5) to produce a best fit
 421 using a 20 nm particle size and M_{Ag} of 2.4 mg L^{-1} (Table 3). The decrease in M_{Ag} from the starting
 422 M_{Ag} (4.3 mg L^{-1}) reflects the potential losses of Ag during sampling and from sorption on to the
 423 solid surfaces of the microcosm. The diffusion coefficient of the modeled particles was 21.5×10^{-12}
 424 m^2s^{-1} exceeding the sedimentation velocity of $0.21 \times 10^{-8} \text{ m s}^{-1}$ (Table 2), evidencing that diffusion
 425 was the dominant migration process. The higher diffusion coefficient confirms diffusion dominated
 426 migration and thus, the maintained stability of the PVP AgNPs when released into the UPW.
 427 Furthermore, the small NP size (20 nm) used to produce the best fit for the modeled Ag
 428 concentration is reflective of the PVP AgNP stability and is comparable to the 'as prepared' PVP-
 429 AgNPs. In addition to the model parameters, the observed total Ag concentration profiles (also
 430 presented in Figures 1A, 1B and 1C) for the UPW conditions, show the Ag concentrations
 431 between each sampled depth were comparable at each time point and satisfy the rules of Stokes-
 432 Einstein Law of particles in solution (Hinderliter, Minard et al. 2010) and Ficks Law of
 433 diffusion (Fick 1855, Gorban, Sargsyan et al. 2011). Therefore, this provides suitable evidence to
 434 support AgNP dissolution. At any given time, the total Ag concentration accounted for >80%
 435 AgNPs and <20% dissolved Ag throughout the study in UPW (Table SI.3).

436 UV-vis is a particularly important tool used to identify changes in AgNP properties, which can
 437 alter their SPR. A single UV-vis peak at 400 nm was comparable to the 'as prepared PVP-AgNPs
 438 (Figure SI.1) showing characteristics of unaltered AgNPs (Tejamaya, Römer et al. 2012), (Römer, White et al. 2011).
 439 Additionally the SPR signal was present for 672 hours (28 days) confirming their presence and

440 stability. TEM imaging (Figures 3A and 3B) also identified small single spherical particles in the
441 surface and bottom depth of the microcosm at 24 hours post release. The average size was 13 ± 7
442 nm in the surface and 14 ± 4 nm in the bottom, showing no significant difference (Table SI.4) when
443 compared to the as prepared PVP-AgNPs prior to release and agrees with the model size fitting
444 parameters. The TEM imaging produced both qualitative and quantitative information which
445 underpins the model concentrations and the UV-vis data to provide strong evidence that PVP-
446 AgNPs remain stable in UPW. These results are also in agreement with previous findings for
447 small sterically-stabilized AgNPs in UPW(Liu and Hurt 2010), therefore diffusion dominated
448 transport was used to show accurate calibrations for the model.

450 3.1.2 Behavior of PVP-AgNPs in MHW

451
452 When the PVP-AgNPs were released into the MHW (Figures 1D, 1E and 1F), the modeled fitting
453 parameters (*ca.* d and M_{Ag}) were appropriate to confirm unaltered particles. The weighted sum of
454 squared errors (Eq 5) optimized the model fits, using a small average size of 14.8 nm (consistent
455 with TEM size analysis) and a M_{Ag} of 2 mg L^{-1} . The optimized model sizes were also comparable
456 to the 'as prepared AgNPs'. The diffusion coefficient of $28.9 \times 10^{-12} \text{ m}^2\text{s}^{-1}$ was higher when
457 compared to the sedimentation velocity of $0.11 \times 10^{-8} \text{ m s}^{-1}$ (Table 3). This information supports
458 that PVP AgNPs maintained stability and migrated through the microcosm columns via diffusion, in
459 a similar fashion to the behavior observed in UPW.

460 It is well documented in the literature that in simple aqueous environments AgNPs form
461 complexes with chloride and sulfide ligands^{(Lowry, Gregory et al. 2012, Tejamaya, Römer et al. 2012,}
462 ^{Peijnenburg, Baalousha et al. 2015),(Levard, Reinsch et al. 2011)}, which were all present in the MHW, although no
463 evidence for their co-existence was found here, in contrast with cit-AgNPs (see section 3.2.2.). In
464 addition, there was some evidence of Ag dissolution and reprecipitation during the study, as 71%
465 of the total Ag concentration was accounted for NPs after 24 hours (Table SI.5), compared to
466 81% on day 28. The co-existence of Ag and Cl present the possibility for precipitation of (most
467 probably) AgCl nanoparticles, as a transformation process (as observed in the EDS profiles in
468 Figure 7B). As AgCl NPs do not have an associated SPR absorbance (Zook, Long et al. 2011), it
469 was not possible to qualitatively identify this association, although the co-existence of the AgCl may
470 explain the slight variations in size.

471 Despite some dissolution and the influence of the water chemistry, a total Ag concentration
472 remained comparable between each depth (surface, middle and bottom) at 120 hours (5 days
473 (Figures 1D, 1E and 1F) and for the duration of the study thereafter.

474 SPR is a good indicator of aggregation of AgNPs(Baalousha, Nur et al. 2013) where additional
475 second absorbance peaks in the region of 500-700 nm confirm the presence of larger
476 particulates(Chinnapongse, MacCuspie et al. 2011, Baalousha, Nur et al. 2013). UV-vis spectra
477 for the PVP-Ag NPs (Figure 2D, 2E, and 2F) show only a single peak in each depth at 400 nm
478 which remains constant for the duration of the study over 672 hours (28 days), which confirms the
479 stability of the PVP-AgNPs. Morphological observations (Figure 3C and 3D) confirm the presence
480 of small spherical particles and measuring 13 ± 8 nm in the surface and 16 ± 6 nm in the bottom
481 post 24 hours release (Table SI.6). These figures are also in agreement to the sized used to fit the
482 model parameters.

484 | 3.1.3 Behavior of PVP-AgNPs in MHW-SRFA

485
486 Evidence for the presence of unaltered PVP-AgNPs in the MHW-SRFA was provided by the
487 optimized model parameters which used particle size of 11 nm and a M_{Ag} of 1.4 mg to create a
488 best fit (Eq 5) between our observed and expected total Ag concentration profiles (Figure 1G, 1H
489 and 1I). The small particle size was comparable to the 'as prepared' PVP-AgNPs and the TEM
490 sizing at 24 hours post release. The model calculated the diffusion coefficient to be $39 \times 10^{-12} \text{ m}^2\text{s}^{-1}$
491 with a sedimentation velocity of $0.06 \times 10^{-8} \text{ m s}^{-1}$ (Table 3). In agreement to the previous water
492 exposures (in UPW) for the PVP-AgNPs, a higher diffusion coefficient strongly suggests that
493 diffusion was the dominant process of migration. Furthermore, evidence to support particle stability
494 and diffusion dominated transport was shown by a maintained concentration gradient between
495 each depth of the mesocosm after 72 hours (days 3), where concentrations of Ag remained
496 comparable at $35 \pm 12 \mu\text{g L}^{-1}$ for the duration of the study. Figure 2G, H and I show the UV-vis
497 absorbance peaks at 400 nm, although the SPR at 300 nm in 2H and 2I is due to interferences of
498 band tailing at 254 nm from the SRFA (USA,EPA, 2009, (Hendricks 2006). UV absorbance
499 spectra show only the absorbance for SRFA is presented in Figure SI.11 (Supporting information).

500 Morphological observations of the PVP-AgNPs at 24 hours post release identified small
501 singular particles (Figure 3E and 3F) sized at 11 ± 3 nm (Table SI.8) at the bottom sampling point.
502 Due to insufficient AgNP numbers for statistical relevance, it was not possible to determine size
503 from the surface sampling point. Nonetheless the reported sizes were comparable to those used
504 to produce a best fit from the model for our data, further confirming PVP-AgNP stability in MHW-
505 SRFA.

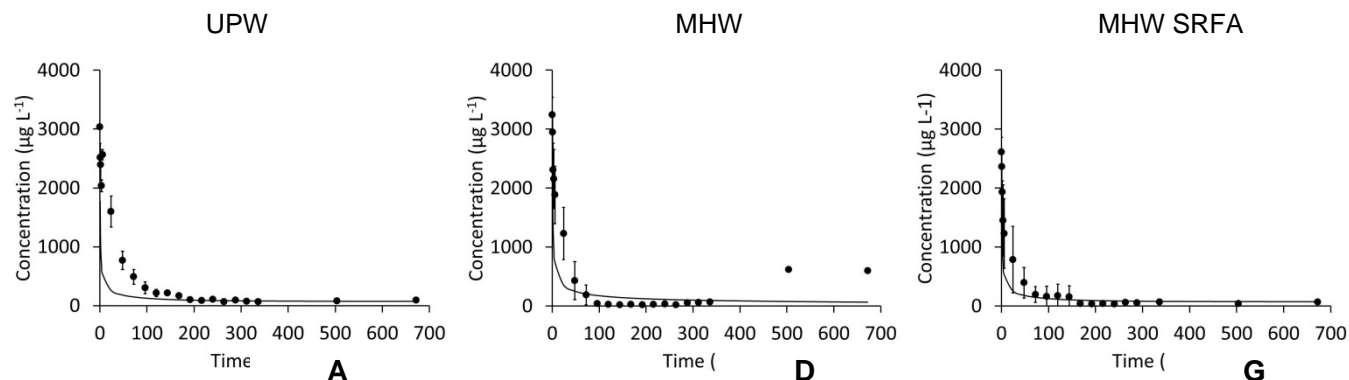
506 To conclude, it is likely that the overall stability of the PVP-AgNPs is due to the
507 thermodynamics of the high molecular weight structural complexity of PVP polymer forming a thick
508 layer that is strongly bound to the surface of the Ag atom(Kvitek, Panáček et al. 2008). Therefore,

509 compared to the citrate surface stabilizer, PVP is not sensitive to charge screening under the
510 influence of the simple electrolyte media, maintaining unaltered AgNPs (Tejamaya, Römer et al. 2012),(Badawy,
511 Luxton et al. 2010), even at high ionic strengths (Kvítek, Panáček et al. 2008),(Ju-Nam and Lead 2008). In addition the
512 stability of the PVP AgNPs in the MHW-SRFA may also have been due to NOM adsorption to the
513 particle surface(Auffan, Bottero et al. 2010, Tejamaya, Römer et al. 2012, Hitchman, Smith et al.
514 2013).

516 *3.2 Behavior and transport of cit-AgNPs*

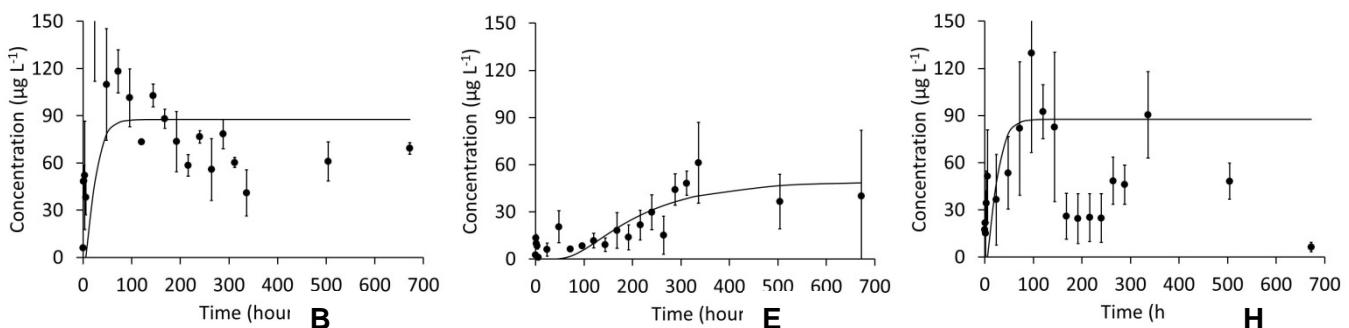
517
518 The observed and modeled Ag concentration profiles for the cit-AgNP releases are presented in
519 Figure 4 for each water condition. The UV-vis profiles are presented in Figure 5 and
520 accompanying TEM imaging for each water condition is shown in Figure 6. In contrast to the PVP-
521 AgNPs (Figure 1), the cit-AgNPs behavior and transport was media-dependant.

545



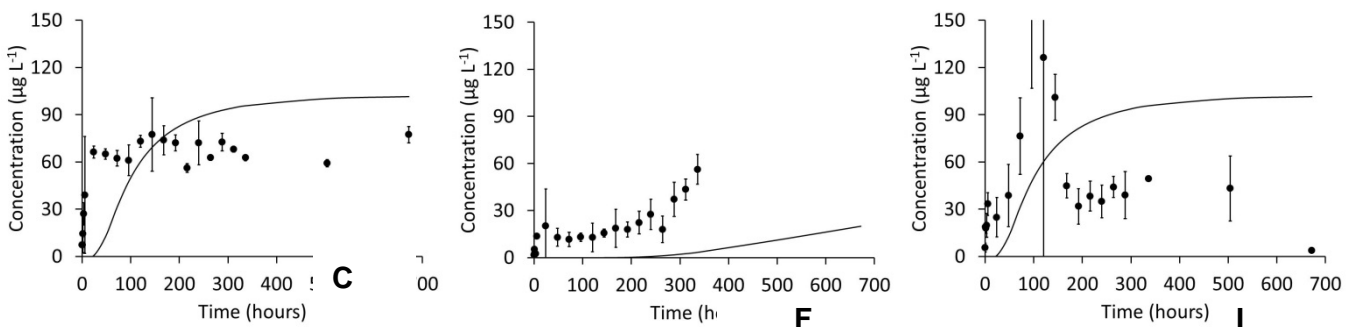
546

Surface



547

Middle



548

Bottom

— Modelled Ag Concentration ● Total Ag Concentration

549

550

Figure 4: Observed and modelled total Ag concentrations over time for the citrate AgNP study in the surface, middle and bottom depths of the mesocosm, in each of the water conditions (parameters in supporting information). A) UPW surface water, B) UPW middle depth water, C) UPW bottom depth water, D) MHW surface water, E) MHW middle depth water, F) MHW bottom

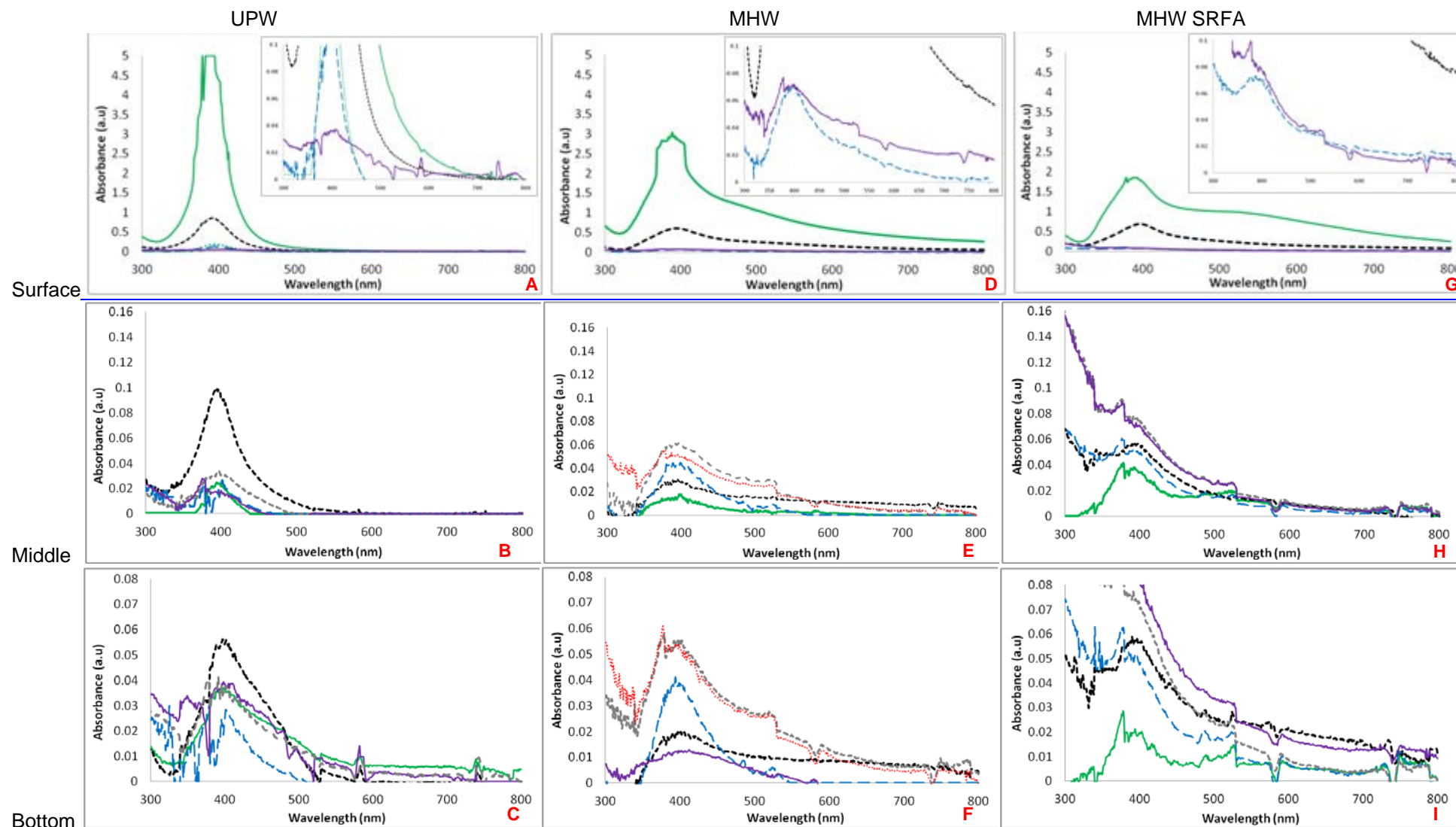
551

552

depth water, G) MHW SRFA surface water, H) MHW SRFA middle depth water and I) MHW SRFA bottom depth water. Dots show the average concentrations of three independent triplicates,

553 error bars represent the standard deviation of the measured concentrations in the three replicated and the solid lines is the fitted model. Mass of Ag NPs introduced to the column fixed at 4.3
554 mg.
555
556

557



558

559

560

561

— 0.5hrs — 24hrs — 120 hrs — 336 hrs 456 hrs — 672 hrs

562
563
564
565
566
567
568
569
570
571
572
573
574
575
576
577
578
579
580
581
582

Figure 5: comparison SPR profiles of citrate AgNP over time for the surface, middle and bottom depths of the mesocosm, in each of the water conditions. A) UPW surface water, B) UPW middle depth water, C) UPW bottom depth water, D) MHW surface water, E) MHW middle depth water, F) MHW bottom depth water, G) MHW SRFA surface water, H) MHW SRFA middle depth water and I) MHW SRFA bottom depth water.

583
584

585

586

587
588
589

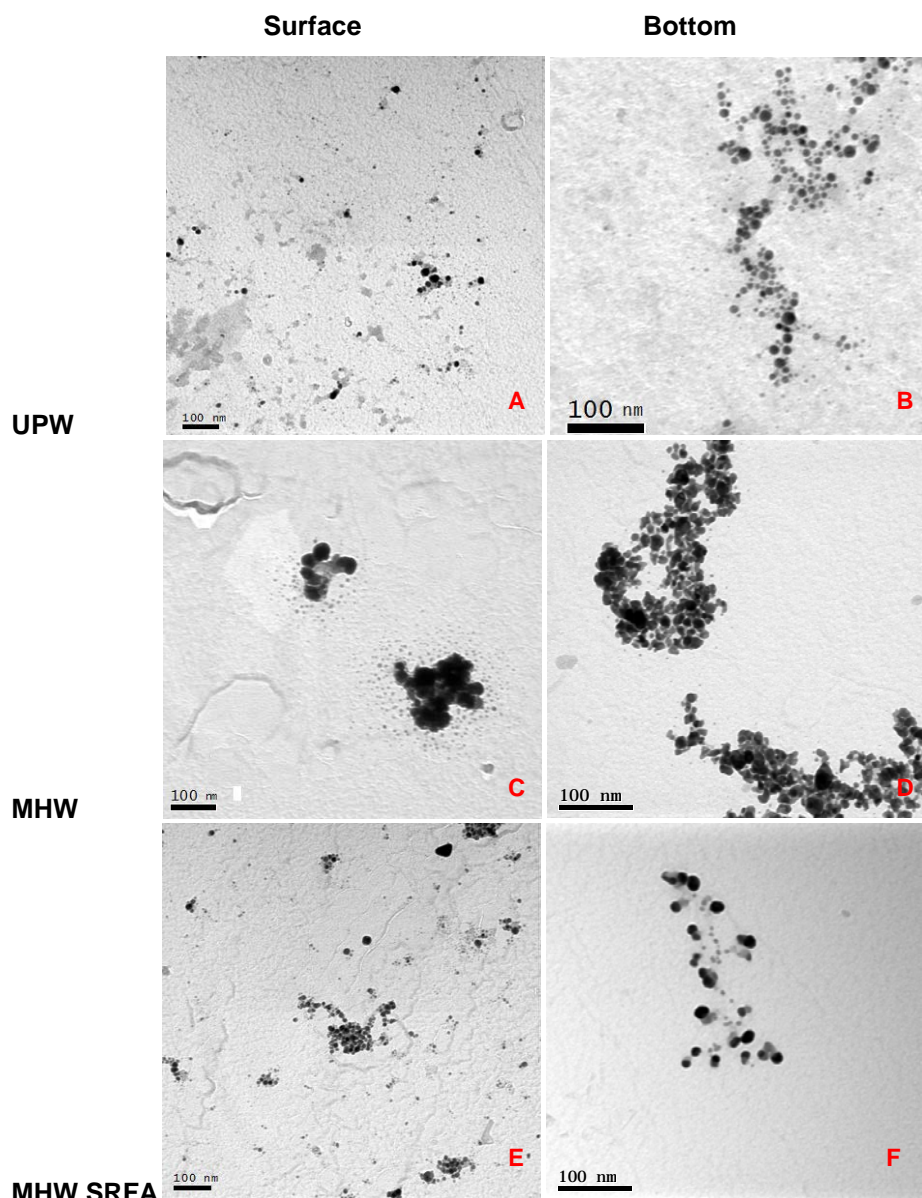


Figure 6: TEM imaging of citrate AgNPs recovered after 24 hours in each of the water conditions, A) surface UPW, B) bottom UPW, C) surface MHW, D) bottom MHW, E) surface MHW SRFA and F) bottom MHW SRFA.

3.2.1 Behavior of cit-AgNPs in UPW

In UPW, the cit-AgNPs remained stable with comparable behavior and transport mechanisms to the PVP-AgNPs, suggesting few transformations in agreement with other studies (Römer, White et al. 2011). To determine stability of the cit-AgNPs the Ag concentration profiles (Figures 4A-C) were fitted (Eq 2), using the weighted square of fitting errors (Eq 5) and the primary particle size of 10 nm with a M_{Ag} of 4 mg. The particle size used was comparable within the error of the measurements to the 'as prepared' cit-AgNPs and in agreement to the TEM sizing (Table SI.4).

The model accurately predicted the total Ag concentrations to identify strong correlations between our observed and expected data using the Chi squared analysis (Eq 5), which were comparable to the PVP-AgNP studies. Table 3 shows a high diffusion coefficient of the 10 nm particles ($43 \times 10^{-12} \text{ m}^2\text{s}^{-1}$) combined with a low settling velocity ($0.05 \times 10^{-8} \text{ m s}^{-1}$), indicating diffusion orientated behaviour of small NPs in suspension. Dissolution of the AgNPs (Table SI.3) was observed after day 1 in each of the surface and bottom of the microcosms, by measuring dissolved and particulate Ag (ultrafiltration). In the surface, the total Ag concentration accounted for 85% AgNPs and 15% dissolved Ag, whereas, the Ag concentration on day 28 accounted for 63% AgNPs and 37% dissolved Ag.

The UV-vis spectra of cit-AgNPs in UPW shows a single absorption peak centered at 392 nm (Figures 5A, 5B and 5C) for each of the surface, middle and bottom depth. These results confirm the stability of the cit-AgNPs in UPW and are consistent with the literature for small spherical particles (Cumberland and Lead 2009), (Tejamaya, Römer et al. 2012), (Römer, White et al. 2011). The UV-vis spectra of cit-AgNPs also identified UV-vis SPR peaks at 672 nm (day 28), confirming AgNP presence in each of the surface, middle and bottom sampling points. Additionally, as discussed in section 2.4, the model inputs do not take into account AgNP dissolution and losses of Ag. Therefore discrepancies between the model and observed total Ag concentration data with the UV evidence can be explained partially by dissolution and sorption. However, since the modeled particle size remains comparable to the 'as prepared' cit-AgNPs (within the error of measurement) the model size values and diffusion coefficient are valid to confirm the cit-AgNPs remain mostly unaltered in UPW. Furthermore, TEM imaging (Figures 6A and 6B) confirmed single spherical particles in the surface and bottom depth of the mesocosm at 24 hours post release, providing evidence to support the model parameters and that the cit-AgNPs migrated via diffusion dominated transport.

3.2.2 Behavior and transport of cit-AgNPs in MHW

624 When introduced to the MHW, the yellow/orange color of the cit-AgNPs immediately changed to
625 dark brown/orange. This became colorless as particles migrated and diluted through the columns
626 over the first 0.5 hours. In the presence of simple electrolytes, the visual color changes on release
627 are consistent with the aggregation of cit-AgNPs^{(Tejamaya, Römer et al. 2012), (Zhang, Smith et al. 2012)}.

628 The modeled concentration profiles for the cit-AgNPs released in MHW, did not fit with the
629 observed Ag concentrations when modeled with the primary particle size as described for the
630 previous UPW study. A larger size of 88.4 nm produced the best fit for the model (Eq 5), further
631 suggesting media-dependent aggregation (and precipitation) and sedimentation behavior, which
632 account for the concentration rises and declines observed in Figures 4D-F (Socolofsky and Jirka
633 2005, Hinderliter, Minard et al. 2010). The settling velocity of the cit-AgNPs also increased to 4
634 $\times 10^{-8} \text{ ms}^{-1}$, whereas the diffusion rate decreased to $4.9 \times 10^{-12} \text{ m}^2\text{s}^{-1}$ (Table 3) evidencing
635 sedimentation dominated migration.

636 Additionally, the total Ag concentration changes over time in the middle and bottom of the
637 microcosm (Figure 4H and 4I), show a systematic trend where the Ag concentration gradually
638 rises to reach a concentration max of $83 \pm 15 \mu\text{g L}^{-1}$ at 336 hours (day 14) before falling to 40 ± 17
639 $\mu\text{g L}^{-1}$ at 504 hours (day 21) and $30 \pm 15 \mu\text{g L}^{-1}$ at 672 hours (day 28) as the Ag begins to settle.
640 The Ag concentration behavior is indicative of both dissolution and precipitation behavior (Table
641 SI.5), combined with sedimentation dominated AgNP transport (i.e. moving as a cloud of
642 aggregated AgNPs through the column). This concentration profile was not observed in the UPW
643 and MHW PVP-AgNP study, indicating surface coating dependent behavior, as well as media
644 dependent behavior.

645 After 14 days, the AgNP concentration accounted for only 54% for the total Ag in the surface
646 water. Similarly, AgNPs only contributed to 57% of the total Ag in the bottom at day 14, with the
647 number being slightly higher due to sedimentation. Reprecipitation of AgNPs was evident in the
648 surface water over time, as the AgNP concentration increased from 65% on day 21 to 71% on day
649 28 (Table SI.5), with no effects to the total Ag concentration. Differences in the cit-AgNP
650 concentration in the surface sampling point over the 28 day study were also accompanied by a
651 reduced SPR peak (Figure 5D), which is consistent with rapid aggregation of cit-Ag
652 NPs(Baalousha, Nur et al. 2013). A UV-vis peak at 392 nm with an additional second absorbance
653 peak in the region of 500-700 nm, also confirmed cit-AgNP instability and aggregation at the
654 surface of the microcosm(Chinnapongse, MacCuspie et al. 2011, Baalousha, Nur et al. 2013).
655 These additional peaks were absent when cit-Ag NPs were released in UPW and for all PVP-
656 AgNP experiments. Furthermore, SPR peaks were only visible in MHW for 456 hours (19 days) in
657 the middle depth compared to 672 hours (28 days) in the UPW exposures, showing a decline in
658 AgNP concentration as they sediment and dissolve.

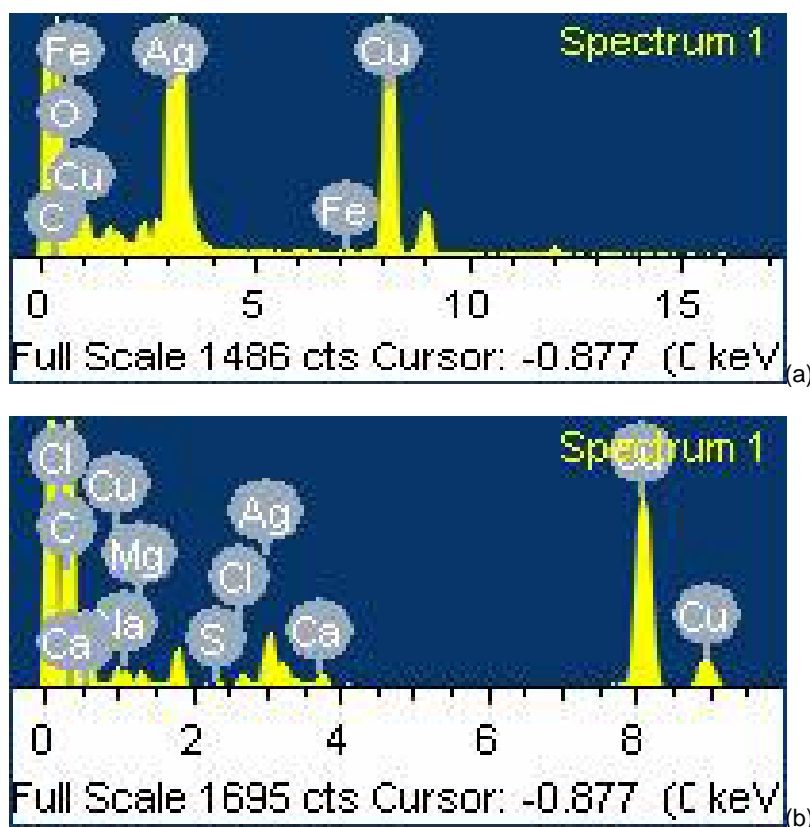
659 TEM imaging revealed that the cit-AgNPs in the surface MHW were 13 ± 5 nm after 24 hours
660 (Figure 6C, Table SI.4) and the cit-AgNPs located at the bottom were significantly larger at 23 ± 23
661 nm (Table SI.6), further evidencing aggregation determined behavior when introduced to an
662 electrolyte containing media. Note that the 88 nm used to model the particle reflects the average
663 core size during the whole time course of the study and does not reflect the changing dissolution
664 and reprecipitation of the NPs. Morphological observations show that the particles were
665 aggregated and larger than those compared to the UPW study at 24 hours in the bottom of the
666 microcosm. EDS (Figure SI.13) confirmed the presence of Ag from the aggregates shown in
667 Figure 6D. The changes that were observed from the TEM imaging between the MHW compared
668 to the UPW are indicative of the physicochemical changes that will incur when exposed to
669 environmental waters.

670 The EDS spectrum (Figures 7B) identified the presence of Ca, Mg, S, Cl and Na in solution, all
671 of which could possibly interact with the charged surface of the cit-AgNPs and thus result in
672 aggregation. Particular interest is given to the presence of divalent cations (Ca^{2+} and Mg^{2+}) shown
673 in Figure 7B, as these have been proven to influence cit-AgNP aggregation by bridging between
674 two anionic molecules. Additionally, aggregation may also have been caused by the cations in
675 solution such as Na and Cl by neutralising surface charge of the citrate stabilizer (Akaighe, Depner
676 et al. 2012). Previous work found that the dilution of AgNPs in media leads to citrate re-
677 equilibration and loss from surface followed by aggregation²⁰, in agreement with the present study
678 which showed the citrate capping to result in more unstable nanoparticles. Differences between
679 UPW and MHW suggests this mechanism (dilution and loss of citrate) is also important. Studies by
680 Baalousha et al, (2013) and Akaighe et al (2012) further observed aggregation of citrate AgNPs in
681 CaCl_2 , MgCl_2 and NaCl_2 containing media ionic strengths relevant to the present study (Akaighe,
682 Depner et al. 2012).

683 Coprecipitation with Cl of the AgNPs is also a possible mechanism that would result in
684 increased aggregation (Levard, Hotze et al. 2012). The results from the present study were also
685 similar to EDS profiles obtained by Ha and Payer (2011) who exposed Ag to a sodium chloride
686 solution (NaCl) and obtained AgCl complexes (Ha and Payer 2011). As citrate coated AgNPs are
687 electrostatically stabilized, they are therefore prone to aggregation by charge neutralization
688 caused by the electrolytes present in the MHW water (Bae, Hwang et al. 2013).

689 As described by the Derjaguin-Landau-Verwey-Overbeek (DLVO) theory, the electrostatic
690 repulsion between two particles in conjunction with van der Waals attraction will determine particle
691 aggregation (Baalousha 2009). Partial removal of the citrate surface coating and a change in the
692 surface charge, induced by ionic strength will reduce the electrostatic diffuse double layer,
693 resulting in increased aggregation (Römer, White et al. 2011). Additionally, UPW does not contain
694 citrate, therefore the re-equilibration of citrate from the NP surface into the aqueous phase, would

695 also result in the surface coating loss. Furthermore, the lack of charge repulsion between the
696 particle surfaces causes decreased charge shielding, susceptibility to dissolution, and the
697 formation of silver complexes with the electrolytes in solution, such as chloride<sup>(Lowry, Gregory et al.
698 2012),(Levard, Reinsch et al. 2011),(Levard, Mitra et al. 2013)</sup>. In contrast, the PVP coated AgNPs are sterically
699 stabilized and are more stable in ionic solutions, as the presence of cations do not significantly
700 influence steric stabilization, or induce charge neutralization.



703
704 Figure 7: A) EDX spectra for pristine citrate AgNP suspensions and B) EDX spectrum for cit-AgNPs located in the surface
705 water after 24 hrs exposure to MHW with additional SRFA. The presence of copper (Cu) and carbon (C) shown in the EDS
706 spectrum represent the carbon film and copper mesh grid used to mount the sample.

708 3.2.3 Behavior of cit-AgNPs in MHW-SRFA

709
710 Using Eq 2, we were able to show the stabilizing effects of SRFA by fitting the model parameters
711 (Figure 4G, 4H and 4I) using the weighted square of fitting errors (Eq 5) with a smaller particle size
712 of 12.7 nm, when compared to the MHW study absent of SRFA. The observed stabilizing effects
713 of cit-AgNPs exposed to low concentrations of NOM are also in agreement with previous
714 literature^{(Chinnapongse, MacCuspie et al. 2011),(Manciualea, Baker et al. 2009)}. The Ag concentration rises over the first
715 5 days (120 hours) in the middle depth (Figure 4H) illustrating sedimentation governed behavior as
716 larger particles settle. However, after 168 hours (7 days) the Ag concentration decreased to $30 \pm$
717 $10 \mu\text{g L}^{-1}$ which remained consistent until the end of the study. This behavior is conformational of a

718 mix of sedimentation and diffusion governed transport mechanisms, despite the smaller modeled
719 size. Additionally this behavior also predicts that the mobility of the cit-AgNPs in natural
720 environments will be influenced by adsorption/deposition onto solid objects such as suspended
721 solids (NOM), soil sediments and organisms, thus reducing their bioavailability and migration
722 (Auffan, Bottero et al. 2010, Bae, Hwang et al. 2013).

723 After 24 hours, the AgNP concentration was higher accounting for 89% of the total Ag in the
724 surface water and 95% in the bottom depth, compared to the previous cit-AgNP studies. The data
725 from Table SI.7 (Supporting Information) suggests the SRFA has reduced the effects of
726 dissolution, although, the higher AgNP concentration in the bottom is indicative of immediate
727 sedimentation, which may have been caused by deposition of the cit-AgNPs on to the SRFA.
728 Aggregation was also confirmed in the UV-vis spectra (Figure 5G,5H and 5I) where a second
729 absorbance peak in the region of 500-700 nm at 0.5 hours was present in the surface
730 water^{(Chinnapongse, MacCuspie et al. 2011),(Baalousha, Nur et al. 2013)}. Aggregation of the cit-AgNPs in the presence
731 of SRFA may be caused by bridging flocculation(Huynh and Chen 2011) and is consistent to
732 findings by Quik et al, 2014 who observed the sedimentation of nanoparticles in a range of natural
733 waters(Quik, Velzeboer et al. 2014). However, the additional second absorbance peaks were no
734 longer present in the middle or bottom depths after this time point, confirming sedimentation and
735 sorption(Bae, Hwang et al. 2013). Additionally, the absence of these UV-vis bands at later
736 sampling points are consistent with the smaller modeled size and previous literature<sup>(Cumberland and
737 Lead 2009),(Tejamaya, Römer et al. 2012)</sup>.

738 NOM has been documented to displace the citrate surface stabilizer by re-coating the particle
739 with NOM (Diegoli, Manciualea et al. 2008) to provide steric stabilization(Baalousha, Manciualea et
740 al. 2008), which has been evidenced in the present study. The steric stabilization from the addition
741 of the SRFA to the MHW enhanced the stability and persistence of the citrate AgNPs in the
742 surface waters by reducing aggregation, which was not observed in the MHW absent of SRFA.
743 Reduced aggregation and sedimentation of the cit-AgNPs was complimented by the reduced SPR
744 banding patterns between 600-800 nm in figures 4G, 4H and 4I after 24 hours, compared the
745 MHW absent of SRFA (Figures 5D, 5E and 5F).

746 Although stabilization of the cit-AgNPs was observed, the formation of aggregates in the
747 presence of SRFA can be explained either by reprecipitation of AgNPs and/or the charge
748 neutralization, charge screening or bridging flocculation(Huynh and Chen 2011) of the SRFA on
749 the AgNP surfaces. SRFA can act as a reducing agent, to nucleate ionic Ag to grown into
750 elemental Ag coated by the NOM (Akaighe, Depner et al. 2012). TEM imaging continued to
751 support the stabilizing effects of the addition of SRFA to the MHW standard (Figure 6E and 6F).
752 The aggregate structure in figures 6E and 6f are morphologically different to those observed in
753 figure 6D, showing small spherical particles closely connected by a surface film similar to those

754 observed in Baalousha et al (2009)(Baalousha 2009), compared to core 'fusion' of the NP
755 aggregates observed in Figure 6d. Cit-AgNPs had an average TEM size of 12 ± 6 nm (Table SI.8)
756 in the surface water comparable to the primary particle size, and were larger in the bottom area at
757 27 ± 10 nm 24 hours post release (Table SI.8: Figure 6E). Results show a reduction in size
758 compared to those observed in the MHW absent of SRFA, demonstrating stability in the presence
759 of NOM.

761 **4 Conclusions**

762 In all conditions, sorption of Ag to the microcosm wall was responsible for Ag concentration
763 losses, suggesting that sorption of particulates might be a dominant behavior when AgNPs are
764 released in to the environment. PVP-AgNPs remained unaltered, regardless of the chemical
765 composition of the water matrix and displayed diffusion dominated transport behaviors. The model
766 data used both the primary 'as prepared' sizes and the reported TEM aggregate sizes (cit-AgNPs)
767 to help validate the transport mechanisms in each study. Further evidence of non-aggregated
768 spherical AgNPs was shown from the TEM imaging and SPR data to support the stability and
769 diffusion of the PVP AgNPs over the citrate AgNPs.

770 Cit-AgNPs were only stable in the UPW studies, whereas ionic concentrations measured in
771 the presence of cit-AgNP indicated complex mass fluctuations, sedimentation dominated migration
772 and potential reprecipitation of AgNP species. These behaviours and transformations are all likely
773 to be dominant when released in real water conditions. The addition of SRFA demonstrated small
774 stabilizing effects to the cit-AgNPs which was validated in the model and TEM imaging where the
775 primary particle sizes compared to the 'as prepared' AgNPs used. The total Ag concentration
776 losses also suggest that eventually the AgNPs will either adsorb to NOM and other surfaces
777 and/or sediment.

778 Based on the information presented in this study we can make predictions that concentrations
779 of AgNPs will be elevated in waters with higher concentrations of NOM, due to the displacements
780 of electrostatic surface coating and sorption of NOM onto the AgNP surface to enhance their
781 stability. AgNPs will also interact with chlorine and sulphur species in natural waters and this may
782 enhance their persistence in environmental conditions. Waters with lower NOM concentrations
783 and higher electrolyte concentrations will favor aggregation mechanisms of electrostatically coated
784 particles and particles with no surface modifications. Aggregated particles will sediment and are
785 likely to be bioavailable to sediment-dwelling organisms with potential implications to this
786 ecological niche.

789 ***Acknowledgments***

790 We would like to thank the Natural Environment Research Council (NE/H013148/1) and the
791 Centre for Environmental Nanoscience and Risk (CENR) for their financial support.

792
793
794
795
796
797
798
799
800
801
802
803
804
805
806
807
808
809
810
811
812
813
814
815
816
817
818
819
820
821
822
823
824
825
826
827
828
829
830
831
832
833
834
835
836
837
838
839
840
841
842
843
844
845
846
847

References

- Akaighe, N., S. W. Depner, S. Banerjee, V. K. Sharma and M. Sohn (2012). "The effects of monovalent and divalent cations on the stability of silver nanoparticles formed from direct reduction of silver ions by Suwannee River humic acid/natural organic matter." Science of the Total Environment **441**: 277-289.
- Auffan, M., J.-Y. Bottero, C. Chaneac and J. Rose (2010). "Inorganic manufactured nanoparticles: how their physicochemical properties influence their biological effects in aqueous environments." Nanomedicine **5**(6): 999-1007.
- Baalousha, M. (2009). "Aggregation and disaggregation of iron oxide nanoparticles: Influence of particle concentration, pH and natural organic matter." Sci Total Environ **407**(6): 2093-2101.
- Baalousha, M., K. Arkill, I. Romer, R. Palmer and J. Lead (2015). "Transformations of citrate and Tween coated silver nanoparticles reacted with Na₂S." Science of The Total Environment **502**: 344-353.
- Baalousha, M. and J. Lead (2012). "Rationalizing nanomaterial sizes measured by atomic force microscopy, flow field-flow fractionation, and dynamic light scattering: sample preparation, polydispersity, and particle structure." Environmental science & technology **46**(11): 6134-6142.
- Baalousha, M. and J. Lead (2013). "Characterization of natural and manufactured nanoparticles by atomic force microscopy: Effect of analysis mode, environment and sample preparation." Colloids and Surfaces A: Physicochemical and Engineering Aspects **419**: 238-247.
- Baalousha, M., A. Manciuola, S. Cumberland, K. Kendall and J. R. Lead (2008). "Aggregation and surface properties of iron oxide nanoparticles: influence of pH and natural organic matter." Environmental Toxicology and Chemistry **27**(9): 1875-1882.
- Baalousha, M., Y. Nur, I. Römer, M. Tejamaya and J. Lead (2013). "Effect of monovalent and divalent cations, anions and fulvic acid on aggregation of citrate-coated silver nanoparticles." Science of the Total Environment **454**: 119-131.
- Badawy, A. M. E., T. P. Luxton, R. G. Silva, K. G. Scheckel, M. T. Suidan and T. M. Tolaymat (2010). "Impact of environmental conditions (pH, ionic strength, and electrolyte type) on the surface charge and aggregation of silver nanoparticles suspensions." Environmental science & technology **44**(4): 1260-1266.
- Bae, S., Y. S. Hwang, Y.-J. Lee and S.-K. Lee (2013). "Effects of water chemistry on aggregation and soil adsorption of silver nanoparticles." Environmental health and toxicology **28**.
- Balnois, E. and K. J. Wilkinson (2002). "Sample preparation techniques for the observation of environmental biopolymers by atomic force microscopy." Colloids and Surfaces A: Physicochemical and Engineering Aspects **207**(1): 229-242.
- Benn, T. M. and P. Westerhoff (2008). "Nanoparticle silver released into water from commercially available sock fabrics." Environmental science & technology **42**(11): 4133-4139.
- Chen, K. L. and M. Elimelech (2007). "Influence of humic acid on the aggregation kinetics of fullerene (C₆₀) nanoparticles in monovalent and divalent electrolyte solutions." Journal of Colloid and Interface Science **309**(1): 126-134.
- Chinnapongse, S. L., R. I. MacCuspie and V. A. Hackley (2011). "Persistence of singly dispersed silver nanoparticles in natural freshwaters, synthetic seawater, and simulated estuarine waters." Science of the total environment **409**(12): 2443-2450.
- Cumberland, S. A. and J. R. Lead (2009). "Particle size distributions of silver nanoparticles at environmentally relevant conditions." Journal of Chromatography A **1216**(52): 9099-9105.
- Dale, A. L., E. A. Casman, G. V. Lowry, J. R. Lead, E. Viparelli and M. Baalousha (2015). "Modeling nanomaterial environmental fate in aquatic systems." Environmental science & technology **49**(5): 2587-2593.
- Diegoli, S., A. L. Manciuola, S. Begum, I. P. Jones, J. R. Lead and J. A. Preece (2008). "Interaction between manufactured gold nanoparticles and naturally occurring organic macromolecules." Science of the Total Environment **402**(1): 51-61.
- Fabrega, J., S. N. Luoma, C. R. Tyler, T. S. Galloway and J. R. Lead (2011). "Silver nanoparticles: behaviour and effects in the aquatic environment." Environment international **37**(2): 517-531.
- Fick, A. (1855). "Ueber diffusion." Annalen der Physik **170**(1): 59-86.
- Gorban, A., H. Sargsyan and H. Wahab (2011). "Quasichemical models of multicomponent nonlinear diffusion." Mathematical Modelling of Natural Phenomena **6**(05): 184-262.
- Gottschalk, F., T. Sun and B. Nowack (2013). "Environmental concentrations of engineered nanomaterials: review of modeling and analytical studies." Environmental Pollution **181**: 287-300.

848 Ha, H. and J. Payer (2011). "The effect of silver chloride formation on the kinetics of silver dissolution in
849 chloride solution." Electrochimica acta **56**(7): 2781-2791.

850 Hendricks, D. W. (2006). Water treatment unit processes: physical and chemical, CRC press.

851 Hinderliter, P. M., K. R. Minard, G. Orr, W. B. Chrisler, B. D. Thrall, J. G. Pounds and J. G. Teeguarden
852 (2010). "ISDD: a computational model of particle sedimentation, diffusion and target cell dosimetry for in
853 vitro toxicity studies." Particle and fibre toxicology **7**(1): 36.

854 Hitchman, A., G. H. S. Smith, Y. Ju-Nam, M. Sterling and J. R. Lead (2013). "The effect of environmentally
855 relevant conditions on PVP stabilised gold nanoparticles." Chemosphere **90**(2): 410-416.

856 Hotze, E. M., T. Phenrat and G. V. Lowry (2010). "Nanoparticle aggregation: challenges to understanding
857 transport and reactivity in the environment." Journal of environmental quality **39**(6): 1909-1924.

858 Huynh, K. A. and K. L. Chen (2011). "Aggregation kinetics of citrate and polyvinylpyrrolidone coated silver
859 nanoparticles in monovalent and divalent electrolyte solutions." Environmental science & technology
860 **45**(13): 5564-5571.

861 Ju-Nam, Y. and J. R. Lead (2008). "Manufactured nanoparticles: an overview of their chemistry,
862 interactions and potential environmental implications." Science of the total environment **400**(1): 396-414.

863 Kvitek, L., A. Panáček, J. Soukupova, M. Kolar, R. Vecerova, R. Prucek, M. Holecová and R. Zboril (2008).
864 "Effect of surfactants and polymers on stability and antibacterial activity of silver nanoparticles (NPs)." The
865 Journal of Physical Chemistry C **112**(15): 5825-5834.

866 La Farre, M., S. Pérez, L. Kantiani and D. Barceló (2008). "Fate and toxicity of emerging pollutants, their
867 metabolites and transformation products in the aquatic environment." TrAC Trends in Analytical Chemistry
868 **27**(11): 991-1007.

869 Levard, C., E. M. Hotze, G. V. Lowry and G. E. Brown Jr (2012). "Environmental transformations of silver
870 nanoparticles: impact on stability and toxicity." Environmental science & technology **46**(13): 6900-6914.

871 Levard, C., S. Mitra, T. Yang, A. D. Jew, A. R. Badireddy, G. V. Lowry and G. E. Brown Jr (2013). "Effect of
872 chloride on the dissolution rate of silver nanoparticles and toxicity to E. coli." Environmental science &
873 technology **47**(11): 5738-5745.

874 Levard, C., B. C. Reinsch, F. M. Michel, C. Oumahi, G. V. Lowry and G. E. Brown Jr (2011). "Sulfidation
875 processes of PVP-coated silver nanoparticles in aqueous solution: impact on dissolution rate." Environmental science & technology **45**(12): 5260-5266.

876 Liu, J. and R. H. Hurt (2010). "Ion release kinetics and particle persistence in aqueous nano-silver colloids." Environmental science & technology **44**(6): 2169-2175.

877 Lowry, G. V., K. B. Gregory, S. C. Apte and J. R. Lead (2012). "Transformations of nanomaterials in the
878 environment." Environmental science & technology **46**(13): 6893-6899.

879 Manciulea, A., A. Baker and J. R. Lead (2009). "A fluorescence quenching study of the interaction of
880 Suwannee River fulvic acid with iron oxide nanoparticles." Chemosphere **76**(8): 1023-1027.

881 Navarro, E., A. Baun, R. Behra, N. B. Hartmann, J. Filser, A.-J. Miao, A. Quigg, P. H. Santschi and L. Sigg
882 (2008). "Environmental behavior and ecotoxicity of engineered nanoparticles to algae, plants, and fungi." Ecotoxicology **17**(5): 372-386.

883 Peijnenburg, W. J., M. Baalousha, J. Chen, Q. Chaudry, F. Von Der Kammer, T. A. Kuhlbusch, J. Lead, C.
884 Nickel, J. T. Quik and M. Renker (2015). "A review of the properties and processes determining the fate of
885 engineered nanomaterials in the aquatic environment." Critical Reviews in Environmental Science and
886 Technology(just-accepted): 00-00.

887 Piccinno, F., F. Gottschalk, S. Seeger and B. Nowack (2012). "Industrial production quantities and uses of
888 ten engineered nanomaterials in Europe and the world." Journal of Nanoparticle Research **14**(9): 1-11.

889 Quik, J., I. Velzeboer, M. Wouterse, A. Koelmans and D. Van de Meent (2014). "Heteroaggregation and
890 sedimentation rates for nanomaterials in natural waters." Water research **48**: 269-279.

891 Römer, I., T. A. White, M. Baalousha, K. Chipman, M. R. Viant and J. R. Lead (2011). "Aggregation and
892 dispersion of silver nanoparticles in exposure media for aquatic toxicity tests." Journal of Chromatography
893 A **1218**(27): 4226-4233.

894 Socolofsky, S. A. and G. H. Jirka (2005). "Special topics in mixing and transport processes in the
895 environment." Engineering—lectures, fifth ed., Coastal and Ocean Engineering Division, Texas A&M
896 University.

897 Tejamaya, M., I. Römer, R. C. Merrifield and J. R. Lead (2012). "Stability of citrate, PVP, and PEG coated
898 silver nanoparticles in ecotoxicology media." Environmental science & technology **46**(13): 7011-7017.

899 Thurman, E. M. (2012). Organic geochemistry of natural waters, Springer Science & Business Media.

900 United States Environmental Protection Agency USA EPA, (2002), "Methods for Measuring the Acute
901 Toxicity of Effluents and Receiving Waters to Freshwater and Marine Organisms", Fifth Edition, **EPA-821-**
902 **R-02-012**

906 United States Environmental Protection Agency USA EPA (2009). "Method 415.3: "Determination of Total
907 Organic Carbon and Specific UV Absorbance at 254 nm in Source Water and Drinking Water." Revision
908 1.2. Document no. **EPA/600/R-09/122**.
909 Zhang, H., J. A. Smith and V. Oyanedel-Craver (2012). "The effect of natural water conditions on the anti-
910 bacterial performance and stability of silver nanoparticles capped with different polymers." Water research
911 **46**(3): 691-699.
912 Zook, J. M., S. E. Long, D. Cleveland, C. L. A. Geronimo and R. I. MacCuspie (2011). "Measuring silver
913 nanoparticle dissolution in complex biological and environmental matrices using UV-visible absorbance."
914 Analytical and bioanalytical chemistry **401**(6): 1993-2002.
915